High Landau levels of two-dimensional electrons near the topological transition caused by interplay of spin-orbit and Zeeman energy shifts

Rajesh K. Malla and M. E. Raikh

Phys. Rev. B **99**, 205426 — Published 21 May 2019

DOI: 10.1103/PhysRevB.99.205426

High Landau levels of 2D electrons near the topological transition caused by interplay of spin-orbit and Zeeman energy shifts

Rajesh K. Malla and M. E. Raikh
Department of Physics and Astronomy, University of Utah, Salt Lake City, UT 84112

In the presence of spin-orbit coupling two branches of the energy spectrum of 2D electrons get shifted in the momentum space. Application of in-plane magnetic field causes the splitting of the branches in energy. When both, spin-orbit coupling and Zeeman splitting are present, the branches of energy spectrum cross at certain energy. Near this energy, the Landau quantization becomes peculiar since semiclassical trajectories, corresponding to individual branches, get coupled. We study this coupling as a function of proximity to the topological transition. Remarkably, the dependence on the proximity is strongly asymmetric reflecting the specifics of the behavior of the trajectories near the crossing. Equally remarkable, on one side of the transition, the magnitude of coupling is an oscillating function of this proximity. These oscillations can be interpreted in terms of the Stückelberg interference. Scaling of characteristic detuning with magnetic length is also unusual. This unusual behavior cannot be captured by simply linearizing the Fermi contours near the crossing point.

PACS numbers:

I. INTRODUCTION

It is known for more than 60 years that, in a metal, the period of the resistance oscillations with magnetic field as well as the period of the oscillations of diamagnetic moment reflect the geometry of its Fermi surface.[1,2] This relation originates from the fact that, by virtue of the Landau quantization, the areas of the cross-sections of the Fermi surface by the planes perpendicular to magnetic field are discrete. These areas are encircled in the course of semiclassical motion of the electron wave packets in magnetic field and contain half-integer number of the flux quanta.

In particular situations when energy gaps, corresponding to neighboring energy bands, are anomalously small, interband tunneling becomes possible. This tunneling, known as magnetic breakdown,[3–6] couples the Fermi surfaces from different bands and modifies the quantization condition to

$$\cos\left(\frac{S_+l^2+S_-l^2}{2}+\varphi_E\right)=\mathcal{T}_E\cos\left(\frac{S_+l^2-S_-l^2}{2}\right), \tag{1}$$

where $S_\pm$ are the areas encircled by the contacting semiclassical trajectories, corresponding to the energy, E, and l is the magnetic length. Parameters $\mathcal{T}_E$ and φ_E are, respectively, the amplitude and the phase of the coupling coefficient between the contacting trajectories. The tunnel probability, $|\mathcal{T}_E|^2$, assumes an appreciable value at energies when the separation of the Fermi surfaces in the momentum space becomes comparable to l^{-1}. Analytical form of $\mathcal{T}_E$ was established[3] using the effective mass approximation, within which the band dispersion near the touching point has the form

$$\varepsilon(\mathbf{k})=\frac{\hbar^2k_x^2}{2m_x}-\frac{\hbar^2k_y^2}{2m_y}, \tag{2}$$

where m_x and m_y are the in-plane effective masses (magnetic field is directed along z). As E crosses from negative to positive values, the connectivity of the Fermi surface, $\varepsilon(\mathbf{k})=E$, changes. In magnetic field, the tunneling probability between the states $k_x\to-\infty$ and $k_x\to\infty$ reduces to the transmission through the "inverted parabola" potential, $-\frac{\hbar^2}{2(m_xm_y)^{1/2}}\left[\frac{(x-k_yl^2)}{l^2}\right]^2$, the result for which, obtained in a celebrated paper by Kemble,[7] reads

$$|\mathcal{T}_E|^2=\frac{1}{\exp\left(-\pi\mu_E\right)+1}, \tag{3}$$

where the parameter μ_E is proportional to energy and is given by $\mu_E=\frac{1}{\hbar^2}\left(m_xm_y\right)^{1/2}El^2$.

Quantization condition Eq. (1) describes topological transitions for spinless electrons with scalar wavefunctions. An alternative scenario of this transition[8–12] unfolds in type-II Weyl semimetals predicted recently[13] and realized experimentally, for review see Refs. 14, 15. In these materials, the contacting contours of the Fermi surface belong to electron and hole pockets, see e.g. Ref. 16. The corresponding states are the eigenfunctions of the matrix Hamiltonian, the simplest version of which has the form[8]

$$\hat{H}_W=ak_x\sigma_0+\sum_i v_ik_i\sigma_i, \tag{4}$$

where σ_0 is a unit matrix and σ_i are the Pauli matrices.

Two branches,

$$E_\pm(\mathbf{k})=ak_x\pm\left[\sum_i v_ik_i^2\right]^{1/2}, \tag{5}$$

of the spectrum defined by the Hamiltonian Eq. (4) touch at the point $\mathbf{k}=0$. The difference between the spectra Eq. (2) and Eq. (5) manifests itself in the expression for the transmission probability. For type-II Weyl semimetals it takes the form[8]

$$|\mathcal{T}_W|^2 = \exp\left(-2\pi\mu_W\right), \tag{6}$$

where μ_W is proportional to the square of minimum separation between the contours and to the square of magnetic length. The origin of the difference between Eqs. (3) and (6) is that the Hamiltonian Eq. (4) allows the Klein tunneling between the electron and hole states. With linear dispersion Eq. (5), the calculation of the tunnel probability reduces to the Landau-Zener problem.

In Ref. 17 it was noted that the topological transition in the geometry of two Fermi contours can be realized for purely two-dimensional electrons subject to in-plane magnetic field and in the presence of spin-orbit coupling. The origin of crossing of the two branches of the spectrum is the interplay of the Zeeman and spin-orbit splittings.[18] The eigenfunctions corresponding to the two crossing branches are spinors. Then it was concluded in Ref. 17 that the semiclassical Landau quantization is governed by Eq. (1) with tunnel probability given by Eq. (6), similarly to the type-II Weyl semimetals.

In the present paper we study in detail the evolution of the 2D Fermi contours in the vicinity of the topological transition emerging in the presence of Zeeman and spin-orbit couplings. We show that, linearizing of the spectrum in the very vicinity of crossing is insufficient to describe the transition probability. Magnetic field dependence of $\mathcal{T}$ as well as its dependence on detuning, is governed by the curvature of the Fermi contours.

II. EVOLUTION OF THE FERMI CONTOURS NEAR THE CROSSING

We start with a 2D Hamiltonian

$$\hat{H} = \frac{\hbar^2 k^2}{2m} + \alpha\left(k_x\sigma_y - k_y\sigma_x\right) - \Delta\sigma_y, \tag{7}$$

where the first term is a free-electron Hamiltonian, while the second and the third terms describe spin-orbit coupling and Zeeman splitting in an in-plane magnetic field, respectively.

Two branches of the spectrum of the Hamiltonian Eq. (7) are given by

$$\mathcal{E}_\pm(\mathbf{k}) = \frac{\hbar^2(k_x^2+k_y^2)}{2m} \pm \left[\left(\Delta - \alpha k_x\right)^2 + \alpha^2 k_y^2\right]^{1/2}. \tag{8}$$

The branches cross at the point

$$k_x = \frac{\Delta}{\alpha}, \quad k_y = 0, \tag{9}$$

which corresponds to the energy

$$\mathcal{E} = \mathcal{E}_0 = \frac{\hbar^2\Delta^2}{2m\alpha^2}. \tag{10}$$

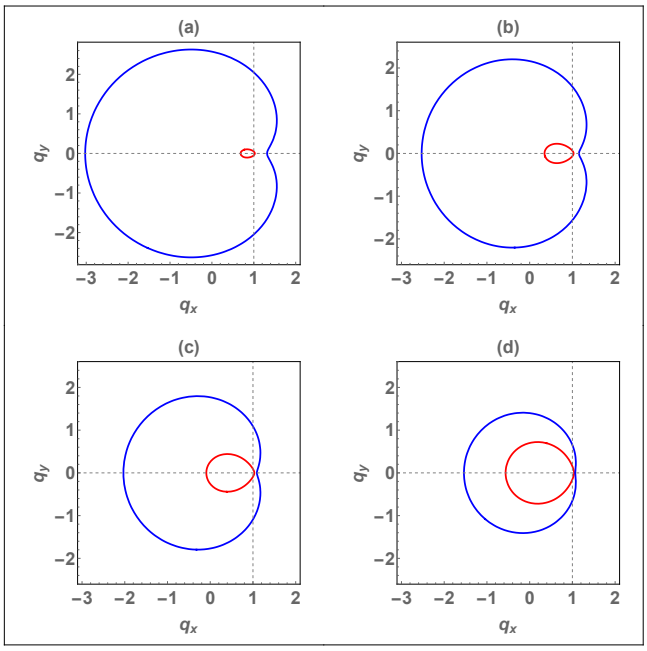

FIG. 1: (Color online) Evolution of the Fermi contours, defined by Eq. (12), with the ratio, ν, of the spin-orbit and Zeeman energy shifts [Eq. (13)]; (a), (b), (c), and (d) correspond to $\nu = 2$, $\nu = 1.5$, $\nu = 1$, and $\nu = 0.5$, respectively. As ν decreases, the inner contour grows. The Fermi energy is chosen to be $\mathcal{E} = 1.1\mathcal{E}_0$ in all panels. Thus, strictly speaking, the separation between the inner and the outer contours is finite at $q_y = 0$. This separation can be distinguished in (a) and (b), but cannot be distinguished in (c) and (d).

To analyze the behavior of the Fermi contours, $\mathcal{E}_\pm(\mathbf{k}) = \mathcal{E}$, we introduce the dimensionless variables

$$k_x = \left(\frac{\Delta}{\alpha}\right)q_x, \quad k_y = \left(\frac{\Delta}{\alpha}\right)q_y, \tag{11}$$

and rewrite Eq. (8) in the form

$$\frac{\mathcal{E}}{\mathcal{E}_0} = q_x^2 + q_y^2 \pm \nu\left[\left(q_x-1\right)^2 + q_y^2\right]^{1/2}, \tag{12}$$

where we have introduced a dimensionless parameter

$$\nu = \frac{2m\alpha^2}{\hbar^2\Delta}, \tag{13}$$

which measures the ratio of the energy shifts due to the spin-orbit and Zeeman couplings.

Near the crossing point $(\mathcal{E} - \mathcal{E}_0) \ll \mathcal{E}_0$ and $q_y \ll 1$ Eq. (12) can be simplified to

$$\left[q_x - 1 - \frac{2\left(\mathcal{E}-\mathcal{E}_0\right)}{\mathcal{E}_0\left(4-\nu^2\right)}\right]^2 - \left(\frac{\nu^2}{4-\nu^2}\right)q_y^2 = \left[\frac{\nu\left(\mathcal{E}-\mathcal{E}_0\right)}{\left(4-\nu^2\right)\mathcal{E}_0}\right]^2. \tag{14}$$

We see that the behavior of the Fermi contours is different for $\nu > 2$ and for $\nu < 2$. For $\nu > 2$ Eq. (14) describes an

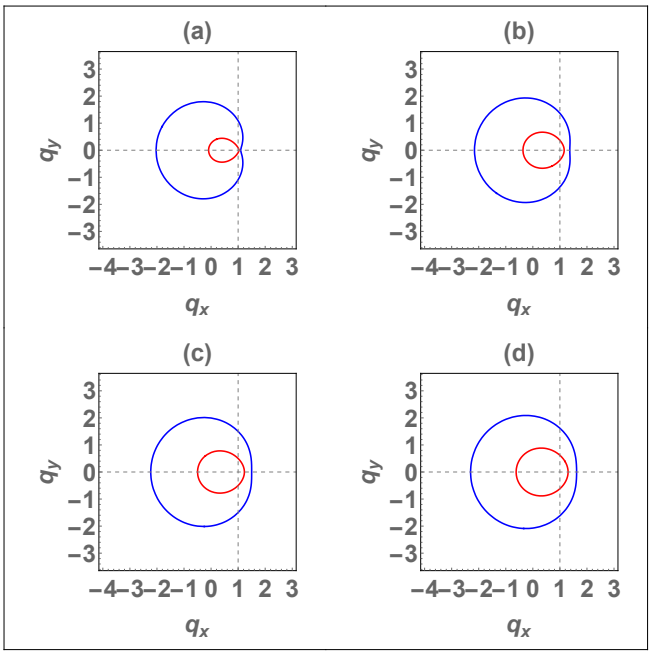

FIG. 2: (Color online) Evolution of the Fermi contours, defined by Eq. (12), with energy. Panels (a), (b), (c), and (d) correspond to energies $\mathcal{E} = 1.1\mathcal{E}_0$, $\mathcal{E} = 1.5\mathcal{E}_0$, $\mathcal{E} = 1.75\mathcal{E}_0$, and $\mathcal{E} = 2\mathcal{E}_0$, respectively. We chose $\nu = 1$ in all panels. It is seen that in panel (c) the outer contour is vertical at $q_y = 0$ in accordance to Eq. (18).

ellipse, i.e. there is only one Fermi contour. For $\nu < 2$ two Fermi contours correspond to the two branches of a hyperbola. There is a real crossing at $\mathcal{E} = \mathcal{E}_0$, namely,

$$q_y = \pm \frac{\left(4-\nu^2\right)^{1/2}}{\nu}(q_x - 1). \tag{15}$$

Evolution of the Fermi contours with ν is illustrated in Fig. 1. It is seen that, as ν decreases below $\nu = 2$, the inner contours grows. The behavior of the outer contour is quadratic near $q_y = 0$ and also at two finite values $\pm\tilde{q}_y$. To find these values, we differentiate Eq. (12) keeping $\mathcal{E}$ constant and obtain

$$\frac{\partial q_x}{\partial q_y} = -\frac{q_y\left\{2\left[\left(q_x-1\right)^2+q_y^2\right]^{1/2} \pm \nu\right\}}{2q_x\left[\left(q_x-1\right)^2+q_y^2\right]^{1/2} \pm \nu(q_x-1)}. \tag{16}$$

The sign "−" corresponds to the outer branch. At $q = \tilde{q}_y$ the derivative turns to zero, which, together with Eq. (12), yields

$$q_x = \tilde{q}_x = \frac{1}{2}\left(1+\frac{\nu^2}{4}+\frac{\mathcal{E}}{\mathcal{E}_0}\right), \tag{17}$$

Substituting this value back into Eq. (12), we find

$$\tilde{q}_y = \frac{1}{2}\left[\left(\frac{\mathcal{E}}{\mathcal{E}_0}+\frac{\nu^2}{4}+\nu-1\right)\left(-\frac{\mathcal{E}}{\mathcal{E}_0}-\frac{\nu^2}{4}+\nu+1\right)\right]^{1/2}. \tag{18}$$

We see that at energy $\frac{\mathcal{E}}{\mathcal{E}_0} = 1+\nu-\frac{\nu^2}{4}$ the outer Fermi contour is vertical at points $(\tilde{q}_x, \pm\tilde{q}_y)$, as illustrated in Fig. 2. At small ν this energy is close to the crossing point of the contours. In magnetic field, this peculiar behavior manifests itself in the coupling between the semiclassical trajectories as we will see in the next Section.

III. TUNNELING BETWEEN THE SEMICLASSICAL TRAJECTORIES

Incorporating magnetic field in the z-direction amounts to replacing k_x by $k_x - \frac{y}{l^2}$. Then the system of equations for the components of the spinor, $(\Psi_1, i\Psi_2)$, takes the form

$$\mathcal{E}\Psi_1 - \frac{\hbar^2}{2m}\left(k_x-\frac{y}{l^2}\right)^2\Psi_1 + \frac{\hbar^2}{2m}\frac{\partial^2\Psi_1}{\partial y^2} = \alpha\left(k_x-\frac{y}{l^2}\right)\Psi_2 - \Delta\Psi_2 + \alpha\frac{\partial\Psi_2}{\partial y}, \tag{19}$$

$$\mathcal{E}\Psi_2 - \frac{\hbar^2}{2m}\left(k_x-\frac{y}{l^2}\right)^2\Psi_2 + \frac{\hbar^2}{2m}\frac{\partial^2\Psi_2}{\partial y^2} = \alpha\left(k_x-\frac{y}{l^2}\right)\Psi_1 - \Delta\Psi_1 - \alpha\frac{\partial\Psi_1}{\partial y}. \tag{20}$$

Upon introducing new functions

$$\Phi_1 = \Psi_1 + \Psi_2, \quad \Phi_2 = \Psi_1 - \Psi_2, \tag{21}$$

and a dimensionless variable

$$u = \frac{\Delta}{\alpha}\left(y - k_x l^2\right) \tag{22}$$

the system can be rewritten as

$$\frac{\mathcal{E}}{\mathcal{E}_0}\Phi_1 + \frac{\partial^2\Phi_1}{\partial u^2} - \left[\left(\frac{\alpha}{\Delta l}\right)^4\left(u+\frac{\Delta}{\hbar\omega_c}\right)^2 - \left(\frac{\nu^2}{4}+\nu\right)\right]\Phi_1 = \nu\frac{\partial\Phi_2}{\partial u}, \tag{23}$$

$$\frac{\mathcal{E}}{\mathcal{E}_0}\Phi_2 + \frac{\partial^2\Phi_2}{\partial u^2} - \left[\left(\frac{\alpha}{\Delta l}\right)^4\left(u-\frac{\Delta}{\hbar\omega_c}\right)^2 - \left(\frac{\nu^2}{4}-\nu\right)\right]\Phi_2 = -\nu\frac{\partial\Phi_1}{\partial u}. \tag{24}$$

Here $\hbar\omega_c = \frac{\hbar^2}{ml^2}$ is the cyclotron energy. Equations (23) and (24) are obtained by adding and subtracting Eqs.

(19) and (20). Square brackets in Eqs. (23) and (24) can be viewed as effective potentials for the functions Φ_1 and Φ_2. These potentials, sketched in Fig. 3 are parabolas shifted horizontally and vertically These potentials cross at

$$u = u_c = \frac{\nu\hbar\omega_c}{2\Delta}\left(\frac{\Delta l}{\alpha}\right)^4 = \left(\frac{\Delta l}{\alpha}\right)^2. \tag{25}$$

The value of potential at $u = u_c$ is equal to

$$\delta = \frac{\mathcal{E} - \mathcal{E}_0}{\mathcal{E}_0}. \tag{26}$$

Parameter δ is the dimensionless measure of the proximity to the crossing. Semiclassical quantization procedure is valid when the Landau levels, corresponding to $\mathcal{E} = \mathcal{E}_0$, are high. Quantitatively, this condition can be expressed as

$$\frac{\mathcal{E}_0}{\hbar\omega_c} = \frac{1}{2}\left(\frac{\Delta l}{\alpha}\right)^2 \gg 1. \tag{27}$$

If the above condition is satisfied, derivation of the equation similar to Eq. (1) for the semiclassical energy levels can be outlined as follows. In the absence of the right-hand sides in Eqs. (23), (24), the solution of (23) represents a wave, incident from the left, which is fully reflected at the turning point (see Fig. 3). The condition that the solution decays to the right from the turning point defines the conventional phase shift, $2\times\frac{\pi}{4}$, between the incident and reflected waves. If the presence of the right-hand side in Eq. (24), there are two channels of reflection: in addition to the reflected-wave solution of Eq. (23), the incident wave can give rise to the solution of (24) propagating to the left, see Fig. 3. If the amplitude of the incident wave is 1, then the amplitude of this second reflected wave should be identified with $\mathcal{T}_E$, the coupling coefficient in the quantization condition Eq. (1). Calculation of $\mathcal{T}_E$ is our main goal. To achieve this goal, it is convenient to analyze the system Eqs. (23), (24) in the momentum space.

In the vicinity of $u = u_c$ the system (23), (24) takes the form

$$\begin{aligned}
\delta\Phi_1 - \mathcal{F}_1 u_1 \Phi_1 + \frac{\partial^2\Phi_1}{\partial u_1^2} &= \nu\frac{\partial\Phi_2}{\partial u_1},\\
\delta\Phi_2 - \mathcal{F}_2 u_1 \Phi_2 + \frac{\partial^2\Phi_2}{\partial u_1^2} &= -\nu\frac{\partial\Phi_1}{\partial u_1},
\end{aligned} \tag{28}$$

where $u_1 = u - u_c$. The slopes $\mathcal{F}_1$, $\mathcal{F}_2$ are defined as

$$\mathcal{F}_1 = 2\Big(\frac{\alpha}{\Delta l}\Big)^2\Big(1+\frac{\nu}{2}\Big), \quad \mathcal{F}_2 = 2\Big(\frac{\alpha}{\Delta l}\Big)^2\Big(1-\frac{\nu}{2}\Big). \tag{29}$$

Upon performing the Fourier transformation in Eq. (28), we arrive to the system of coupled first-order differential equations for the transformed functions Φ_1 and Φ_2

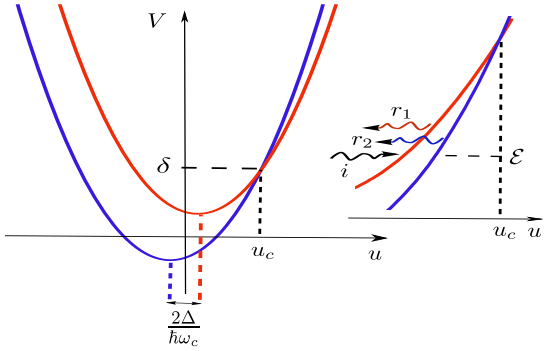

FIG. 3: (Color online) Without the right-hand sides, Eqs. (23) and (24) are decoupled and describe the electron motion in parabolic potentials (blue and red, respectively). The potentials cross at $u = u_c$. Without coupling, the incident wave, i, see inset is fully reflected into the wave, r_1, propagating in the red parabola. With right-hand sides caused by spin-orbit coupling, another channel of reflection into the wave r_2 propagating in the blue parabola emerges. The corresponding reflection probability should be identified with transmission probability $|\mathcal{T}_E|^2$.

$$\begin{aligned}
\delta\tilde\Phi_1 - i\mathcal{F}_1\frac{\partial\tilde\Phi_1}{\partial\kappa} - \kappa^2\tilde\Phi_1 &= i\nu\kappa\tilde\Phi_2,\\
\delta\tilde\Phi_2 - i\mathcal{F}_2\frac{\partial\tilde\Phi_2}{\partial\kappa} - \kappa^2\tilde\Phi_2 &= -i\nu\kappa\tilde\Phi_1.
\end{aligned} \tag{30}$$

To analyze this system, it is convenient to "antisymmetrize" it by eliminating the symmetric phase. This is achieved by introducing instead of $\tilde\Phi_1$, $\tilde\Phi_2$ the new functions defined as

$$\tilde\Upsilon_{1,2}(\kappa) = \tilde\Phi_{1,2}(\kappa)\exp\left[-i\left(\delta\kappa - \frac{\kappa^3}{3}\right)\frac{\mathcal{F}_1+\mathcal{F}_2}{2\mathcal{F}_1\mathcal{F}_2}\right]. \tag{31}$$

Then the system Eq. (30) assumes the form

$$\begin{aligned}
i\mathcal{F}_1\frac{\partial\tilde\Upsilon_1}{\partial\kappa} + \frac{\mathcal{F}_1-\mathcal{F}_2}{2\mathcal{F}_2}\left(\delta-\kappa^2\right)\tilde\Upsilon_1 &= i\nu\kappa\tilde\Upsilon_2,\\
i\mathcal{F}_2\frac{\partial\tilde\Upsilon_2}{\partial\kappa} - \frac{\mathcal{F}_1-\mathcal{F}_2}{2\mathcal{F}_1}\left(\delta-\kappa^2\right)\tilde\Upsilon_2 &= -i\nu\kappa\tilde\Upsilon_1.
\end{aligned} \tag{32}$$

The product $\nu\kappa$ in the right-hand sides describes the coupling between the semiclassical trajectories. We will first assume that the coupling is weak and find the transmission coefficient perturbatively. In the zeroth order we neglect the right-hand side in the first equation, so that

$$\tilde\Upsilon_1(\kappa) = \exp\left[i\frac{\mathcal{F}_1-\mathcal{F}_2}{2\mathcal{F}_1\mathcal{F}_2}\left(\delta\kappa - \frac{\kappa^3}{3}\right)\right]. \tag{33}$$

Substituting $\tilde\Upsilon_1(\kappa)$ into the second equation and solving for $\tilde\Upsilon_2(\kappa)$ we find

$$|\tilde\Upsilon_2(\infty)|^2 = \frac{\nu^2}{\mathcal{F}_2^2}\left|\int_{-\infty}^{\infty} d\kappa\ \kappa\exp\left[i\frac{\mathcal{F}_1-\mathcal{F}_2}{\mathcal{F}_1\mathcal{F}_2}\left(\delta\kappa-\frac{\kappa^3}{3}\right)\right]\right|^2. \tag{34}$$

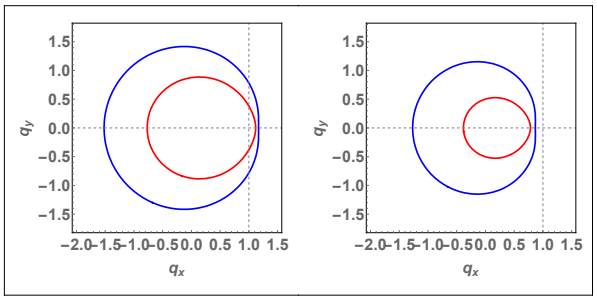

FIG. 4: (Color online) Illustration of the asymmetry of the Fermi-contours with respect to the sign of detuning, δ. In the left panel the contours are shown for $\delta = 0.3$, while in the right panel for $\delta = -0.3$. Parameter ν is chosen to be 0.4 for both panels. Despite the seemingly small difference between the two panels, the transmission coefficient, $|\mathcal{T}_E|^2$, in the right panel is much smaller than in the left panel.

The meaning of $|\tilde{\Upsilon}_2(\infty)|^2$ is the power transmission coefficient, $|\mathcal{T}_\mathcal{E}|^2$, analogously to Eq. (3).

It is easy to see that only the imaginary part of the exponent contributes to the integral. Then the integral reduces to the derivative of the Airy function, $Ai(z)$. Using the expressions for $\mathcal{F}_1$, $\mathcal{F}_2$ we rewrite the final result in the form

$$|\mathcal{T}_\mathcal{E}|^2 = 4\pi^2 \left(\frac{\nu}{2}\right)^{2/3} \left(\frac{\Delta l}{\alpha}\right)^{4/3} \left| Ai'\left[-\delta \left(\frac{\nu}{2}\right)^{2/3} \left(\frac{\Delta l}{\alpha}\right)^{4/3}\right]\right|^2. \tag{35}$$

Our prime observation is that the coupling is an asymmetric function of the detuning, δ. This, actually, reflects the asymmetry of the Fermi-contours' arrangement with respect to the sign of δ. The situation is illustrated in Fig. 4, where the Fermi contours are plotted for $\delta = 0.3$ and $\delta = -0.3$. At negative δ the transmission probability falls off with $|\delta|$ as $\exp\left[-\frac{2}{3}|\delta|^{2/3}\nu\left(\frac{\Delta l}{\alpha}\right)^2\right]$. Note that, by contrast to Eqs. (3) and (6), characteristic δ scales with magnetic field as $l^{-4/3}$, instead of l^{-2} and l^{-1}, respectively.

It is seen from Eq. (35) that at positive δ the transmission coefficient oscillates with δ. Unfortunately, Eq. (35) obtained perturbatively, is not applicable in this domain. This is because it predicts that $|\mathcal{T}_\mathcal{E}|^2$ exceeds 1 at large positive δ. For this reason, in the next Section we turn to numerics.

IV. NUMERICAL RESULTS

For numerical calculations it is convenient to perform a rescaling, $\kappa = Gz$, in the system Eq. (32), where the parameter G is equal to

$$G = \left(\frac{2}{\nu}\right)^{1/2} \left(\frac{\alpha}{\Delta l}\right) = \frac{\hbar\omega_c}{\Delta}. \tag{36}$$

Then the system assumes the form

$$i\tilde{\Upsilon}_1' + \frac{1}{2}\left(\frac{\delta}{G} - Gz^2\right)\tilde{\Upsilon}_1 = iz\tilde{\Upsilon}_2,$$
$$i\tilde{\Upsilon}_2' - \frac{1}{2}\left(\frac{\delta}{G} - Gz^2\right)\tilde{\Upsilon}_2 = -iz\tilde{\Upsilon}_1. \tag{37}$$

We see that, effectively, the transmission coefficient depends only on two parameters, detuning δ and the dimensionless magnetic field, G^2. For numerical purposes it is convenient to get rid of the fast oscillations of $\tilde{\Upsilon}_1$ and $\tilde{\Upsilon}_2$ by introducing new variables

$$\rho_{1,2} = \tilde{\Upsilon}_{1,2} \exp\left[\mp\frac{i}{2}\left(\frac{\delta}{G}z - G\frac{z^3}{3}\right)\right]. \tag{38}$$

With these new variables the oscillating functions appear in the coupling of ρ_1 and ρ_2, namely

$$i\frac{\partial\rho_1}{\partial z} = iz\exp\left[-i\left(\frac{\delta}{G}z - G\frac{z^3}{3}\right)\right]\rho_2,$$
$$i\frac{\partial\rho_2}{\partial z} = -iz\exp\left[i\left(\frac{\delta}{G}z - G\frac{z^3}{3}\right)\right]\rho_1. \tag{39}$$

In terms of parameter G, the result Eq. (35) reads

$$|\mathcal{T}_\mathcal{E}|^2 = |\rho_2(\infty)|^2 = \frac{4\pi^2}{G^{4/3}}\left|Ai'\left(-\frac{\delta}{G^{4/3}}\right)\right|^2. \tag{40}$$

In our numerical calculations we first analyzed the behavior of $|\rho_{1,2}|^2$ with z. In general these quantities exhibit oscillations on the background of a smooth envelop. There is way to approximately isolate this envelop. To do so, we integrate the second equation of the system Eq. (39) using the condition $\rho_2(-\infty) = 0$ and substitute the expression for $\rho_2(z)$ into the first equation. This yields the following closed integral-differential equation for $\rho_1(z)$

$$\frac{\partial\rho_1}{\partial z} = z\int_{-\infty}^{z} dz' z' \rho_1(z') \exp\left\{i\left[\frac{\delta}{G}(z-z') - \frac{G}{3}\left(z^3 - z'^3\right)\right]\right\}. \tag{41}$$

The procedure of extracting the envelop from this equation is developed in Ref. 19. Employing this procedure yields

$$|\rho_1(z)|^2 = \frac{\left(\frac{\delta}{G} - Gz^2\right)^2}{z^2 + \left(\frac{\delta}{G} - Gz^2\right)^2}. \tag{42}$$

The derivation of Eq. (42) is briefly outlined in the footnote Ref. 20.

In Fig. 5 we plot $|\rho_2(z)|^2$ for two values of detuning $\delta = 3$ (upper panel) and $\delta = -3$ (lower panel) with $G = 1$. Apparently the smooth part of $\delta = -3$ curve agrees with theoretical prediction Eq. (42) much better than the smooth part of $\delta = 3$ curve. The reason for this

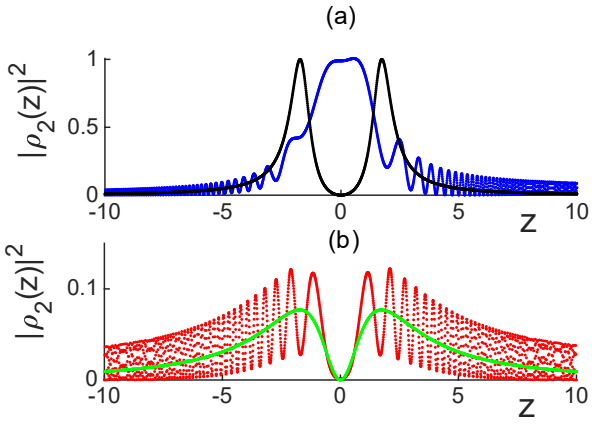

FIG. 5: (Color online) Numerical solution, $|\rho_2(z)|^2$, of the system Eq. (20) is plotted for two values of detuning $\delta = 3$ (a) and $\delta = -3$ (b) and for $G = 1$. The black line in (a) and the green line in (b) are the envelops plotted from Eq. (42). We see that the agreement with theory is much better in (b), since Eq. (42) neglects interference.

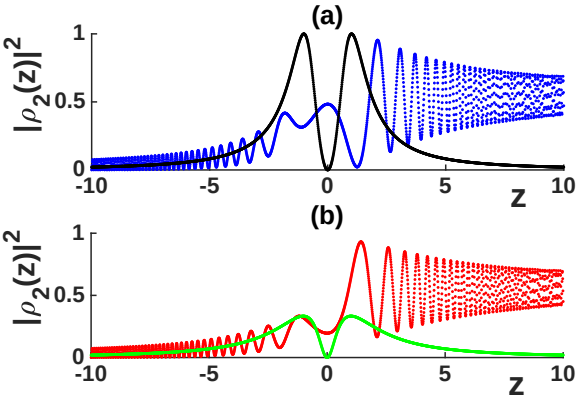

FIG. 6: (Color online) Numerical solution, $|\rho_2(z)|^2$, of the system Eq. (20) is plotted for two values of detuning $\delta = 0.5$ (a) and $\delta = -0.5$ (b) and for $G = 0.7$. The black line in (a) and the green line in (b) are the envelops plotted from Eq. (42). We see that $|\rho_2(z)|^2$ approaches finite values at large z. This approach is accompanied by huge oscillations which complicate the determination of the transmission coefficient.

is obvious: Eq. (42) does not capture the interference between the virtual transitions at negative and positive z. This interference, having the same origin as Stükelberg oscillations takes place at positive δ. Since δ in Fig. 5 was chosen to be big, the values of $\rho_2(z)$ approach zero at large z. To capture the finite transmission, we chose the parameters $G = 0.7$ and $\delta = \pm 0.5$, and plotted $|\rho_2(z)|^2$ in Fig. 6. The agreement with Eq. (42) is worse in Fig. 6 since, for chosen parameters, the regime of transmission is less "semiclassical". We also see that approaching of $|\rho_2(z)|^2$ to finite values at large z is accompanied by huge oscillations. These oscillations introduce an uncertainty in the value $|\rho_2(\infty)|^2$ due to necessary averaging. This uncertainty manifests itself as wiggles in the dependencies of $|\rho_2(\infty)|^2$ on G and δ to which we now turn.

For zero detuning, the theoretical prediction for the transmission coefficient is

$$|\rho(\infty)|^2 = \frac{2.645}{G^{4/3}}, \tag{43}$$

as follows from Eq. (40). In Fig. 7 we plot this G-dependence together with $|\rho(\infty)|^2(G)$ obtained numerically. We observe the agreement with theory at large G, where the theory is applicable. Concerning the theoretically relevant small-G domain, numerical errors did not allow us to establish the G-dependence at very small G. It can be concluded that the averaged over strong oscillations transmission coefficient approaches $\frac{1}{2}$ at small G and has a maximum near $G = 1$. We discuss the theoretical prediction for $|\rho(\infty)|^2(G)$ at small G in the next Section.

Finally, we studied numerically the dependence of the transmision coefficient on detuning, δ. The result is shown in Fig. 8 for the value of $G = 1.5$. We see that for negative δ, the numerics agrees quite well with the theo-

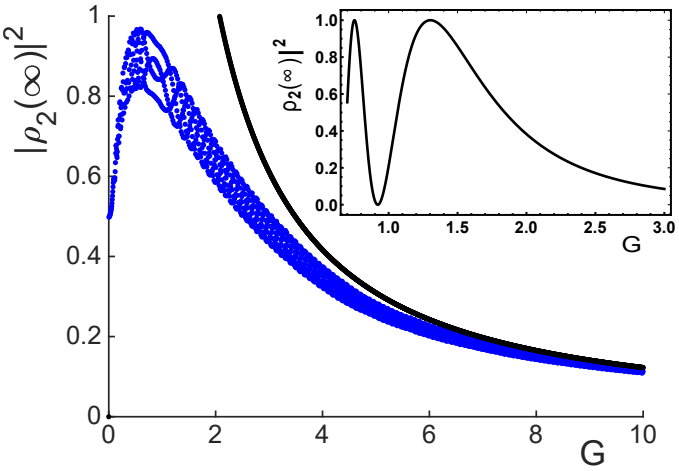

FIG. 7: (Color online) Blue curve, which shows the transmission coefficient obtained numerically, is plotted versus dimensionless magnetic field, G, directly at topological transition $\delta = 0$. Black curve, which shows theoretical prediction for transmission coefficient, is plotted from Eq. (43). In the inset we plot the prediction, $\sin^2(\frac{8}{3G^2})$, based on heuristic argument given in Section V.

retical prediction Eq. (40). For large positive δ, Eq. (40), strictly speaking, does not apply, but qualitative agreement is apparent. Oscillatory behavior of the transmission coefficient is the consequence of the Stückleberg interference of virtual Landau-Zener transitions taking place at $z = \pm\frac{\delta^{1/2}}{G}$.

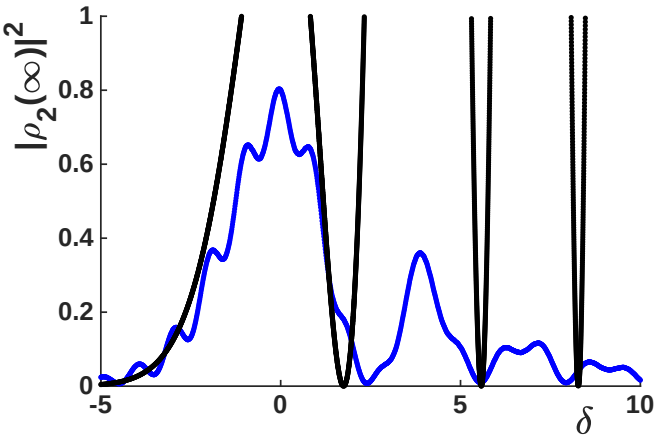

FIG. 8: (Color online) Transmission coefficient (blue curve) obtained numerically is plotted versus the detuning, δ, for dimensionless magnetic field $G = 1.5$. Theoretical prediction for transmission coefficient (black curve) is plotted from Eq. (40). Small wiggles in the numerical curves are the artifact of the averaging procedure. For negative detunings the agreement with theory is good. For positive detunings, theory predicts oscillations with magnitude bigger than 1, while in numerical curve these oscillations, manifesting the Stückelberg interference,[21] slowly decrease with δ.

V. DISCUSSION

(i) It is instructive to compare our analysis to Ref. 17, where it was concluded that the probability $|\mathcal{T}_E|^2$ is given by the Landau-Zener formula. Obviously, the Landau-Zener result is a consequence of linearization of the two branches near their crossing point. The criterion for this linearization given in Ref. 17 is that the cyclotron energy is small enough. In our notations, this criterion can be written as $\Delta \gg \frac{\hbar^2}{ml^2}$, which is nothing but the requirement that $G \ll 1$, where parameter G is defined by Eq. (36).

In order to check this criterion, let us trace how the Landau-Zener formula might emerge from our system Eq. (30)

In the semiclassical limit, the solutions $\tilde{\Upsilon}_1$, and $\tilde{\Upsilon}_2$ of the system Eq. (30) are proportional to $\exp[i\sigma(\kappa)]$, where the derivative of the action, $\sigma(\kappa)$, is given by

$$\sigma'(\kappa) = \pm\frac{\mathcal{F}_1 - \mathcal{F}_2}{2\mathcal{F}_1\mathcal{F}_2}\left[\left(\delta - \kappa^2\right)^2 + \frac{4\nu^2\mathcal{F}_1\mathcal{F}_2}{\left(\mathcal{F}_1 - \mathcal{F}_2\right)^2}\kappa^2\right]^{1/2}. \tag{44}$$

Using Eq. (29), we specify the combinations in the square brackets and in the prefactor

$$\frac{4\nu^2\mathcal{F}_1\mathcal{F}_2}{\left(\mathcal{F}_1 - \mathcal{F}_2\right)^2} = (4 - \nu^2), \quad \frac{\mathcal{F}_1 - \mathcal{F}_2}{2\mathcal{F}_1\mathcal{F}_2} = \left(\frac{\Delta l}{\alpha}\right)^2 \frac{2\nu}{4 - \nu^2}. \tag{45}$$

It seems that for small $\delta \ll 1$ the term κ^2 can be dropped from $(\delta - \kappa^2)^2$. Indeed, if this term is dropped, the expression in the square brackets turns to zero at $\kappa = \pm i\kappa_-$, where

$$\kappa_- \approx \frac{\delta}{\left(4 - \nu^2\right)^{1/2}} \approx \frac{\delta}{2}. \tag{46}$$

Since $\kappa_-^2 = \frac{\delta^2}{4}$ is much smaller than δ, dropping κ^2 is justified. Once δ^2 is dropped, the expression for $\sigma'(\kappa)$ assumes the standard Landau-Zener form with transition probability given by: $\exp\left[-\frac{\pi\nu\delta^2}{8}\left(\frac{\Delta l}{\alpha}\right)^2\right]$. This is the result obtained in Ref. 17.

In our opinion, the domain of applicability of this result is limited for the following reason. In addition to $\kappa = \pm i\kappa_-$, Eq. (44) turns to zero at $\kappa = \pm i\kappa_+$, where $\kappa_+ \approx \left(4 - \nu^2\right)^{1/2} \approx 2$. The point κ_+ originates from the second derivatives, $\frac{\partial^2\Phi_1}{\partial u_1^2}$, $\frac{\partial^2\Phi_1}{\partial u_1^2}$, in Eq. (28) which accounts for the curvature of the spectrum neglected in Ref. 17. The value κ_+ is much bigger than δ and depends on detuning only weakly. This suggests that $\mathcal{T}_E$ is the result of a "two-stage" process: one involving big momentum transfer $\sim \kappa_+$ and another involving small momentum transfer, $\sim \kappa_-$. The resulting $\mathcal{T}_E$ is a strongly oscillating function of detuning and magnetic field. In fact, similar situation, i.e. numerous complex zeros in σ', was encountered in Refs. 22–27.

Returning to Ref. 17, we conclude that, the criterion $G \ll 1$ is not sufficient. For Landau-Zener result to apply, the detuning, δ, and the degree of degeneracy, ν, cannot be both small. This can be derived from the above analysis. Indeed, the values κ_+ and κ_- merge for $\delta = 1 - \frac{\nu^2}{4}$, so that either δ is not small, or the value of ν is close to 2. It also follows from the perturbative result Eq. (40) that for small G the detuning must be appreciable.

(ii) Overall, we were not able to capture the most relevant domain where both δ and G are small neither analytically nor numerically. This is due to strongly oscillating character of $|\rho_2(z)|^2$. The physical origin of this complication is that simple linearizng the Fermi contours near the crossing is insufficient for finding the transition probability. The amplitudes $\rho_1(z)$ and $\rho_2(z)$ keep "talking" to each other outside the domain where linearization applies. Below we present a heuristic account of the behavior of the transmission coefficient at zero detuning. Conventionally,[28] the transmission coefficient in the Landau-Zener problem can be found upon setting κ in the expression for $\sigma'(\kappa)$ to be purely imaginary and integrating between two turning points. This procedure is applicable when the resulting action is big, so that the transmission is small. If we adopt this procedure in Eq. (44) after setting $\delta = 0$, we would realize that, unlike for the Landau-Zener transition, the action is *imaginary* and is equal to

$$i\sigma = \int_{-2/G}^{2/G} dz \left[z^2 - \frac{G^2 z^4}{4}\right]^{1/2} = \frac{8}{3G^2}. \tag{47}$$

We see that at small G the magnitude of action is big and that the transmission coefficient *oscillates* with G instead of being exponentially small. We cannot judge about the prefactor, except that in Landau-Zener transition the prefactor is 1. This leads to the prediction $|\rho_2(\infty)|^2 = \sin^2(\frac{8}{3G^2})$. This prediction is plotted in the inset of Fig. 7. A maximum at $G = 1.3$ can possibly account for the behavior of the numerical curve around $G \sim 1$. If the above heuristic argument applies, then the δ-dependence of the transmission at small G should be weak.

(*iii*) The result Eq. (35) can be derived directly from the system Eq. (28) without transforming to the momentum space. The zeroth-order solution of the first equation is $Ai\left[\frac{1}{\mathcal{F}_1^{1/3}}\left(\delta\mathcal{F}_1 - u_1\right)\right]$. Thus, the right-hand side in the second equation is the derivative of the Airy function. Forced solution of the second equation contains the overlap of this right-hand side with the free solution of the second equation, which is $\Phi_2(u_1) = Ai\left[\frac{1}{\mathcal{F}_2^{1/3}}\left(\delta\mathcal{F}_2 - u_1\right)\right]$. Then the result Eq. (35) follows from the identity

$$\int\limits_{-\infty}^{\infty} dx Ai\left[\lambda(x-a)\right] Ai'\left[\mu(x-b)\right] = \frac{\pi\lambda}{\left(\lambda^3-\mu^3\right)^{2/3}} Ai'\left[\frac{\lambda\mu(a-b)}{\left(\lambda^3-\mu^3\right)^{1/3}}\right], \qquad (48)$$

which can be easily verified using the integral representation of the Airy function.

VI. CONCLUSION

On the qualitative level, the result of this paper can be summarized as follows. In the conventional theory of the topological transition the electron motion in the momentum space can be separated into the propagation along the Fermi contours and the "beatings" between the contours in the region where these contours nearly touch. This separation applies when the domain of "beatings" is much smaller than the size of the Fermi contours. For a particular situation of two crossing spin-orbit sub-bands, considered in this paper, the two contours do not depart after crossing but stay close, i.e. remain nearly degenerate. The stronger is this degeneracy, the less applicable is the separation into propagation and beating. In other words, the the domain of beating occupies progressively bigger portion of the Fermi contours. Crudely speaking, the transmission coefficient oscillates around $|\mathcal{T}_E|^2 = \frac{1}{2}$ when sub-bands are almost degenerate. The oscillations of $|\mathcal{T}_E|^2$ depend strongly on the magnetic field, so that the other sources of the magnetic-field dependence, see e.g. Ref. 29, relevant away from the transition can be neglected.

VII. ACKNOWLEDGEMENTS

This work was supported by the Department of Energy, Office of Basic Energy Sciences, Grant No. DE-FG02-06ER46313.

[1] L. Onsager, "Interpretation of the de Haas-van Alphen Effect," Philos. Mag. **43**, 1006 (1952).

[2] I. M. Lifshitz and A. M. Kosevich, "Theory of magnetic susceptibility in metals at low temperatures," Sov. Phys. JETP **2**, 636 (1956).

[3] G. E. Zil'berman, "Electron in a periodic electric and homogeneous magnetic field, II," Sov. Phys. JETP **6**, 299 (1958).

[4] M. Ya. Azbel, "Quasiclassical quantization in the neighborhood of singular classical trajectories," Sov. Phys. JETP **12**, 891 (1961).

[5] A. A. Slutskin, "Dynamics of Conduction Electrons under Magnetic Breakdown Conditions," Sov. Phys. JETP **26**, 474 (1968).

[6] M. I. Kaganov and A. A. Slutskin, "Coherent magnetic breakdown," Phys. Rep. **98**, 189 (1983).

[7] E. C. Kemble, "A Contribution to the Theory of the B.W. K. Method," Phys. Rev. **48**, 549 (1935).

[8] T. E. O'Brien, M. Diez, and C. W. J. Beenakker, "Magnetic Breakdown and Klein Tunneling in a Type-II Weyl Semimetal," Phys. Rev. Lett. **116**, 236401 (2016).

[9] A. Alexandradinata and L. Glazman, "Modern theory of magnetic breakdown," Phys. Rev. Lett. **119**, 256601 (2017).

[10] A. Alexandradinata and L. Glazman, "Semiclassical theory of Landau levels and magnetic breakdown in topological metals," Phys. Rev. B **97**, 144422 (2018).

[11] A. Alexandradinata, C. Wang, W. Duan, and L. Glazman, "Revealing the Topology of Fermi-Surface Wave Functions from Magnetic Quantum Oscillations," Phys. Rev. X **8**, 011027 (2018).

[12] D. R. Saykin, K. S. Tikhonov, and Ya. I. Rodionov, "Landau levels with magnetic tunneling in a Weyl semimetal and magnetoconductance of a ballistic p-n junction," Phys. Rev. B **97**, 041202(R) (2018).

[13] A. A. Soluyanov, D. Gresch, Z. Wang, Q.-S. Wu, M. Troyer, X. Dai, and B. A. Bernevig, "Type-II Weyl Semimetals," Nature **527**, 495 (2015).

[14] N. P. Armitage, E. J. Mele, and A. Vishwanath, "Weyl and Dirac semimetals in three-dimensional solids," Rev. Mod. Phys. **90**, 015001 (2018).

[15] P. K. Das, D. Di Sante, F. Cilento, C. Bigi, D. Kopic, D. Soranzio, A. Sterzi, J. A. Krieger, I. Vobornik, J. Fujii, T. Okuda, V. N. Strocov, M. B. H. Breese, F. Parmigiani, G. Rossi, S. Picozzi, R. Thomale, G. Sangiovanni, R. J. Cava, G. Panaccione, "Electronic properties of type-II Weyl semimetal WTe_2. A review perspective," arXiv:1812.07215.

[16] Y. Wu, N. H. Jo, M. Ochi, L. Huang, D. Mou, S. L. Bud'ko, P. C. Canfield, N. Trivedi, R. Arita, and A. Kaminski, "Temperature-Induced Lifshitz Transition in WTe_2," Phys. Rev. Lett. **115**, 166602 (2015).

[17] C. Wang, W. Duan, L. Glazman, and A. Alexandradinata "Landau quantization of nearly degenerate bands, and full symmetry classification of avoided Landau-level crossings," arXiv:1810.01908.

[18] R. Glenn, O. A. Starykh, and M. E. Raikh, "Interplay of spin-orbit coupling and Zeeman splitting in the absorption lineshape of fermions in two dimensions," Phys. Rev. B **86**, 024423 (2012).

[19] R. K. Malla, E. G. Mishchenko, and M. E. Raikh, "Suppression of the Landau-Zener transition probability by a weak classical noise," Phys. Rev. B **96**, 075419 (2017).

[20] To derive Eq. (42) from Eq. (41), we note that the strong oscillations of the exponent suggest that the major contribution to the integral comes from the domain $(z-z') \ll z$. To make use of this relation, one should transform the integral in right-hand side by parts. After that, the derivative $\frac{\partial \rho_1}{\partial z'}$ should be taken out of the integral at $z = z'$. This leads to a first order differential equation for $\rho_1(z)$, the solution of which is given by Eq. (42).

[21] S. N. Shevchenko, S. Ashhab, and F. Nori, "Landau-Zener-Stckelberg interferometry," Phys. Rep. **492** 1(2010).

[22] C. Zhu and H. Nakamura, "Theory of nonadiabatic transition for general twostate curve crossing problems. I. Nonadiabatic tunneling case," J. Chem. Phys. **101**, 10630 (1994).

[23] C. Zhu and H. Nakamura, "Theory of nonadiabatic transition for general two-state curve crossing problems. II. Landau-Zener case," J. Chem. Phys. **102**, 7448 (1995).

[24] L.-K. Lim, J.-N. Fuchs, and G. Montambaux, "Bloch-Zener Oscillations across a Merging Transition of Dirac Points," Phys. Rev. Lett. **108**, 175303 (2012).

[25] J.-N. Fuchs, L.-K. Lim, and G. Montambaux, "Interband tunneling near the merging transition of Dirac cones," Phys. Rev. A **86**, 063613 (2012).

[26] L.-K. Lim, J.-N. Fuchs, and G. Montambaux, "Mass and Chirality Inversion of a Dirac Cone Pair in Stckelberg Interferometry," Phys. Rev. Lett. **112**, 155302 (2014).

[27] L.-K. Lim, J.-N. Fuchs, and G. Montambaux, "Geometric phase in Stückelberg interferometry," Phys. Rev. A **91**, 042119 (2015).

[28] A. M. Dykhne, "Adiabatic perturbation of discrete spectrum states," Sov. Phys. JETP **14**, 941 (1962).

[29] Y. Gao and Q. Niu, "Zero-Field Magnetic Response Functions in Landau Levels," Proc. Natl. Acad. Sci.U.S.A. **114**, 7295 (2017).